

Effect of uniform distributions of bonded and debonded fibers on the growth of the fiber/matrix interface crack in UD laminates with different fiber contents under transverse loading

Luca Di Stasio^{a,b}, Janis Varna^b, Zoubir Ayadi^a

^aUniversité de Lorraine, EEIGM, IJL, 6 Rue Bastien Lepage, F-54010 Nancy, France

^bLuleå University of Technology, University Campus, SE-97187 Luleå, Sweden

Abstract

Priority: 1

Target journal(s): Composites Part B: Engineering, Composites Part A: Applied Science and Manufacturing, Composite Structures, Journal of Composite Materials, Composite Communications

1. Introduction

1. We start with a few lines devoted to the spread tow technology and thin plies: what they are, what can be done, what are the possible applications.
- 5 2. By quoting the relevant references, we report on the observation that one of the main beneficial mechanisms in thin ply is the retardation of transverse crack propagation. We then enlarge by reporting the microscopical observations by Saito, in which debonds where also observed. We observe that available microscopic observations are just a few and mainly in 2D.
- 10 3. Propagation of transverse cracks has been widely investigated both analytically and numerically
4. Initiation at the level of fiber/matrix interface is instead a less researched subject.

5. cohesive elements are a possible choice, but have some drawbacks, which
15 makes a LEFM approach valuable
6. With regard to LEFM studies of laminates under transverse loading, models can be found in the literature about: the single fiber in infinite matrix under different mode of loading, the effect of adjacent fibers on a fiber in infinite matrix under different mode of loading, the single fiber in an
20 equivalent composite in transverse tension, the effect of adjacent fibers on a fiber in an equivalent composite in transverse tension.
7. For initiation of transverse cracking at the fiber/matrix interface in UD laminates under transverse tension, there is thus a gap regarding: the effect of fiber volume fraction; the interaction of debonded and bonded
25 fibers in micro-structured assemblies, i.e. no homogenization. This article addresses these two points.
8. We conclude the introduction with a summary of the article's structure.

2. RVE models & FE discretization

2.1. Introduction & Nomenclature

30 In order to investigate the interaction between debonds in UD composites, we developed different models of laminates in which the only damage present is represented by the fiber/matrix interface crack. All of these Representative Volume Elements feature regular microstructures with fibers placed according to a square-packing tiling. As the very high longitudinal modulus of UD composites and cross-ply laminates ensures that the y-strain due to loading in the
35 x-direction is small, we consider only 2D models under the assumption of plane strain, defined in the $x - z$ section of the laminate. Consequently, debonds are considered to be significantly longer in the fiber direction than in the arc direction. The analysis presented thus applies to long debonds, of which we
40 are interested in understanding the mechanisms of growth along its arc direction. The UD composites are further supposed to be subjected to transverse

tension, applied along the x direction in the pictures. As the models are differentiated by the number of layers of fibers and by the spacing between debonds along the vertical and horizontal directions, we introduce the common notation

45 $D(m+1)H(k+1)V(2p+1)L$ which stands for: *a **D**ebond every $(m+1)^{th}$ fiber in the **H**orizontal direction and every $(k+1)^{th}$ fiber in the **V**ertical direction, in a UD composites with $(2p+1)^{th}$ **L**ayers of fibers.* The exact meaning of the parameters m , k , and p will become clearer in Section 2.2.

2.2. Models of Representative Volume Element (RVE)

50 The first two models feature, as shown in Fig. 1, a UD laminate with only one layer of fibers across its thickness. This is quite an extreme model from the microstructural point of view; however, it allows to focus the analysis on the interaction between debonds placed along the direction of the load. Furthermore, as the upper surface is considered free, the interaction is stronger in this case

55 than in any other, making the predictions of this model rather conservative. In retrospective, if only 20 years ago such a model would have been considered too abstracted from the physical reality, the recent advancements in the spread tow technology make this approach appealing also for practical considerations.

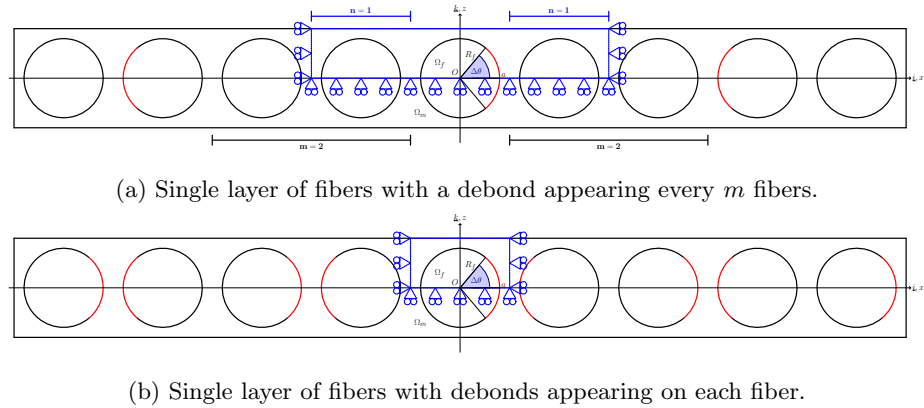


Figure 1: Models of UD laminates with a single layer of fibers and debonds repeating at different distances. The corresponding repeating element (RVE) is highlighted in blue.

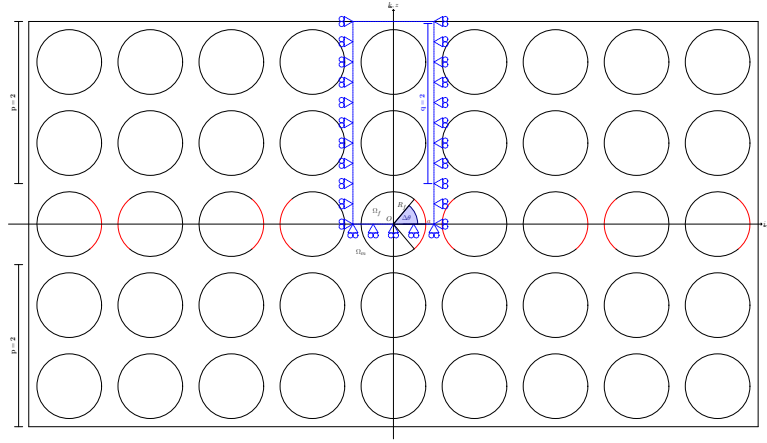
In the first version of the model laminate, Fig. 1a, debonds appear in the

60 laminate on every $(m+1)^{th}$ fiber on alternating sides of the partially debonded
 fiber. The symmetries of the model allow the use of a Repeating Unit Cell
 (RUC), which corresponds to the Representative Volume Element (RVE) of this
 microstructure, with a central debonded fiber and $n = \frac{m}{2}$ fiber(s) on each side.
 It is highlighted by blue lines in 1a. Symmetry is applied on the lower boundary
 65 and kinematic coupling conditions on the left and right sides. As mentioned,
 the upper surface is left free. Following the notation introduced in Section 2.1,
 we will refer to this model as $D(m+1)H0V1L$, where $k = -1, p = 0$. In
 the second version of the single-layer-of-fibers model, 1b, a debond appears on
 each fiber on alternating sides. The corresponding RUC has only one debonded
 70 fiber, with symmetry on the lower side and kinematic coupling on the left and
 right ones. The upper boundary is again free. We will refer to this model as
 $D1H0V1L$, where $k = -1, m = p = 0$.

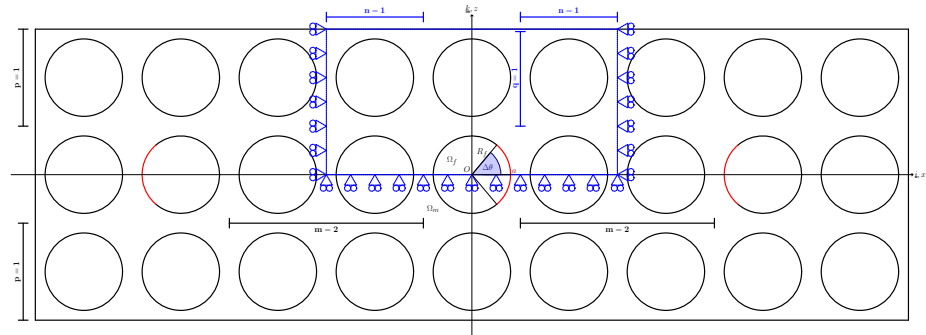
The second set of models considers instead laminates with multiple layers of
 fibers across the thickness: a finite number of layers in the first two models (2a
 75 and 2b); an infinite number in the model of Fig. 3. In the first model (Fig. 2a)
 all the fibers in the central layer are debonded. The UD is made by $2p+1$
 layers of fibers across the thickness, corresponding to a RUC with $q = p$ fibers
 above. This model will be referred to in the following as $D1H0V(2p+1)L$,
 where $k = -1, m = 0$. In the second model (Fig. 2b), a debond appear every
 80 $(m+1)^{th}$ fiber in the central line of fibers in a laminate with $2p+1$ layers. The
 corresponding RUC has thus $n = \frac{m}{2}$ fiber(s) on each side and $q = p$ above. We
 will refer to this model as $D(m+1)H0V(2p+1)L$, where $k = -1$.

Finally, the last model considers an UD composite with an infinite number
 of partially debonded fibers. The corresponding RUC is made by a single fiber
 85 with a debond and kinematic coupling conditions applied to the upper boundary.
 This model is referred to as $D1H1V\infty L$, where $m = k = 0, p \rightarrow \infty$. For all
 these last three models, the corresponding RUC possesses symmetry on the
 lower boundary, and kinematic coupling is applied on the left and right sides.

A summary of models' names and characteristics is reported in Table 1



(a) Multiple layers of fibers with debonds appearing on each fiber belonging to the central layer.



(b) Mutiple layers of fibers with a debond appearing every m fibers within the central layer.

Figure 2: Models of UD laminates with different layers of fibers and debonds repeating at different distances. The corresponding repeating element (RVE) is highlighted in blue.

90 2.3. Finite Element (FE) discretization

Each RUC is discretized using the Finite Element Method (FEM) within the Abaqus environment, a commercial FEM package [1]. The length l and height h of the model (see Fig. 4a) are determined by number of fibers n present on the side and the number of layers q above the central line of fibers (see 2.2)

95 according to Eq. 1:



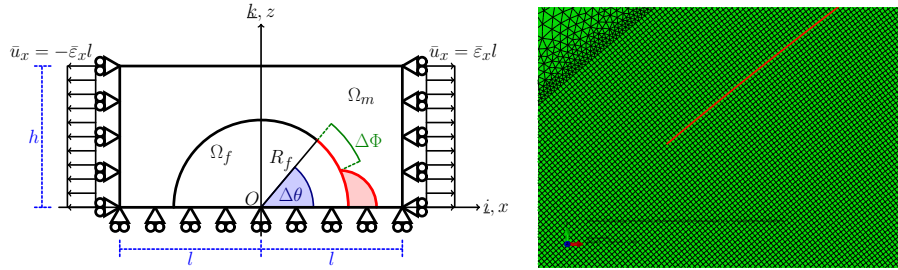
Figure 3: Model of UD laminates with an infinite number of layers of fibers and debonds appearing on each fiber. The corresponding repeating element (RVE) is highlighted in blue.

$$l = (2n + 1) L \quad h = (2q + 1) L; \quad (1)$$

where the reference length L is defined as a function of the fiber volume fraction V_f and the fibers' radius according to

$$L = \frac{R_f}{2} \sqrt{\frac{\pi}{V_f}}. \quad (2)$$

The fibers' radius R_f is assumed to be the same for each fiber present in the model and equal to $1\mu m$. The relationships in Eqs. 1 and 2 thus ensure that the local and global V_f are everywhere equal.



(a) Schematic of the model with its main parameters. (b) Mesh near the crack tip. Crack's faces shown in red.

Figure 4: Details and main parameters of the Finite Element model.

The debond is placed symmetrically with respect to the x axis (in red in 4a)

Table 1: Summary of the models and their characteristics.

Name	Boundary conditions			
	Up	Down	Right	Left
D(m + 1)H0V1L	x-symmetry	free	coupling, $\bar{\varepsilon}_x = 1\%$	coupling, $\bar{\varepsilon}_x = 1\%$
A debond every $(m + 1)^{th}$ fiber in the horizontal direction, in a UD composites with 1 layer of fibers, Fig. 1a.				
D1H0V1L	x-symmetry	free	coupling, $\bar{\varepsilon}_x = 1\%$	coupling, $\bar{\varepsilon}_x = 1\%$
A debond every 1^{st} fiber in the horizontal direction, in a UD composites with 1 layer of fibers, Fig. 1b.				
D1H0V(2p + 1)L	x-symmetry	free	coupling, $\bar{\varepsilon}_x = 1\%$	coupling, $\bar{\varepsilon}_x = 1\%$
A debond every 1^{st} fiber in the horizontal direction, in a UD composites with $(2p + 1)$ layer of fibers, Fig. 2a.				
D(m + 1)H0V(2p + 1)L	x-symmetry	free	coupling, $\bar{\varepsilon}_x = 1\%$	coupling, $\bar{\varepsilon}_x = 1\%$
A debond every $(m + 1)^{th}$ fiber in the horizontal direction, in a UD composites with $(2p + 1)$ layers of fibers, Fig. 2b.				
D1H1V∞L	x-symmetry	coupling	coupling, $\bar{\varepsilon}_x = 1\%$	coupling, $\bar{\varepsilon}_x = 1\%$
A debond every 1^{st} fiber in the horizontal direction and every 1^{st} fiber in the vertical direction, in a UD composites with an infinite number of layers of fibers, Fig. 3.				

and has an angular size of $\Delta\theta$ (the full debond's size is thus $2\Delta\theta$). For high debond's sizes ($\geq 60^\circ - 80^\circ$), a region of variable size $\Delta\Phi$ appears at the crack tip in which the crack's faces are in contact and slide on each other. Due to its appearance, frictionless contact is considered between the two crack's faces

105

to allow free slipping and avoid interpenetration. Symmetry with respect to the x axis is applied on the lower boundary and kinematic coupling on the left and right sides. The upper boundary is in general free, except for the model $D1H1V\infty L$ (Fig. 3) which requires kinematic coupling also on the upper side.

110 Constant transverse strain $\bar{\varepsilon}$ equal to 1% is applied to the right and left sides by means of an imposed displacement of, respectively, $\pm\bar{\varepsilon}l$.

Table 2: Summary of the mechanical properties of fiber and matrix.

Material	E [GPa]	G [GPa]	ν [–]
Glass fiber	70.0	29.2	0.2
Epoxy	3.5	1.25	0.4

The model is meshed using second order, 2D, plane strain triangular (CPE6) and rectangular (CPE8) elements. A regular mesh of quadrilateral elements with an almost unitary aspect ratio is required at the crack tip, as shown in

115 Fig. 4b. The angular size δ of an element in the crack tip region is always equal to 0.05° . The mode I, mode II and total Energy Release Rates (ERRs) represent the main output of the FEM analysis; they are evaluated using the VCCT technique [2] implemented in a custom Python routine and, for the total ERR, the J-integral [3] by application of the Abaqus built-in functionality. A

120 glass fiber-epoxy system is considered in every model, and it is assumed that their response lies always in the linear elastic domain. The properties used are listed in Table 2.

2.4. Validation of the model

The model is validated in Fig. 5 against the results reported in [4], obtained

125 with the Boundary Element Method (BEM) for a single fiber with a symmetric debond placed in an infinite matrix. This situation is modeled using the *free* RVE with $V_f = 0.0079\%$, which corresponds to a RUC's length and height of ~ 100 .

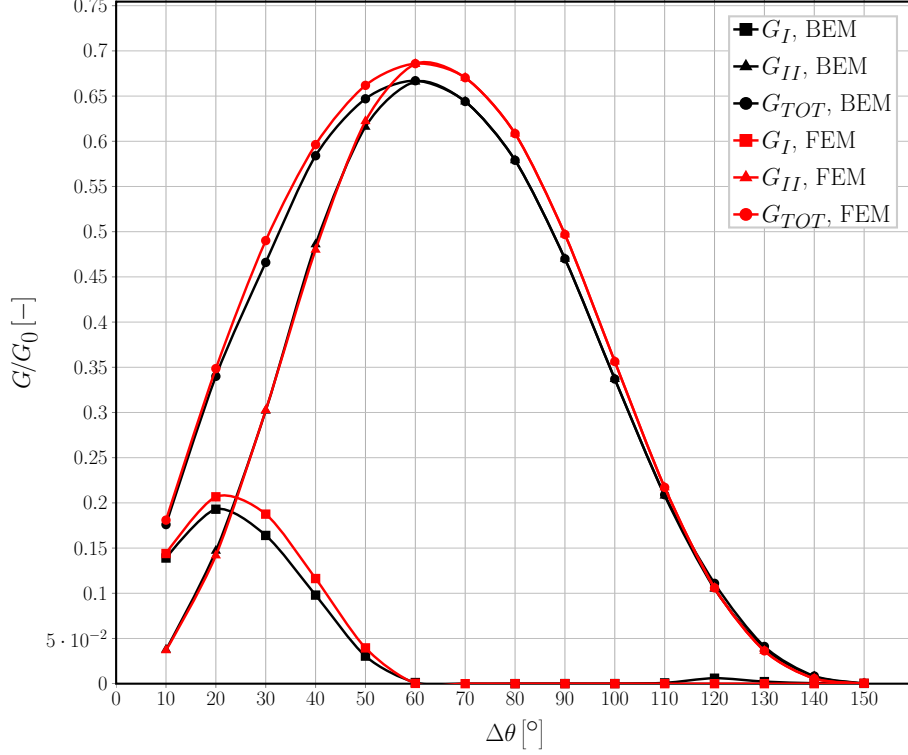


Figure 5: Validation of the single fiber model for the infinite matrix case with respect to the BEM solution in [4].

To allow for a comparison, the results are normalized following [4] with
 130 respect to a reference Energy Release Rate G_0 defined as

$$G_0 = \frac{1 + k_m}{8\mu_m} \sigma_0^2 \pi R_f \quad (3)$$

where μ is the shear modulus, k_m is the Kolosov's constant defined as $3 - 4\nu$
 for plane strain conditions, R_f is the fiber radius and the pedix m refers to
 the properties of the matrix. σ_0 is the stress at the boundary, computed as
 the average of the stress extracted at each boundary node along the right side
 135 (arithmetic average as nodes are equispaced by design along both the left and
 right sides).

3. Results & Discussion

3.1. Effect of Fiber Volume Fraction

The effect is similar for all the different BC cases, it's enough to show some of them to exemplify. G_I in Fig. 6, G_{II} in Fig. 7.

Graphics of ERR vs $\Delta\theta$, one curve for each V_f , one graphic for each selected BC. Selected BC: free, coupling, some examples with fibers (see captions).

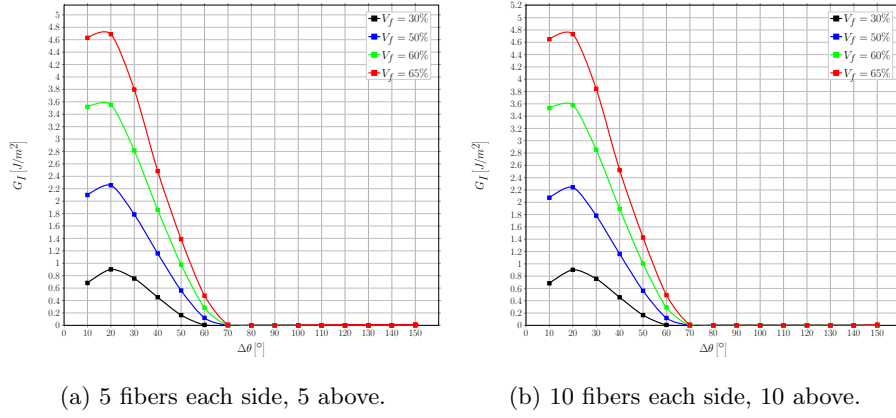


Figure 6: A view of the effect of fiber volume fraction on Mode I ERR in two exemplificative models.

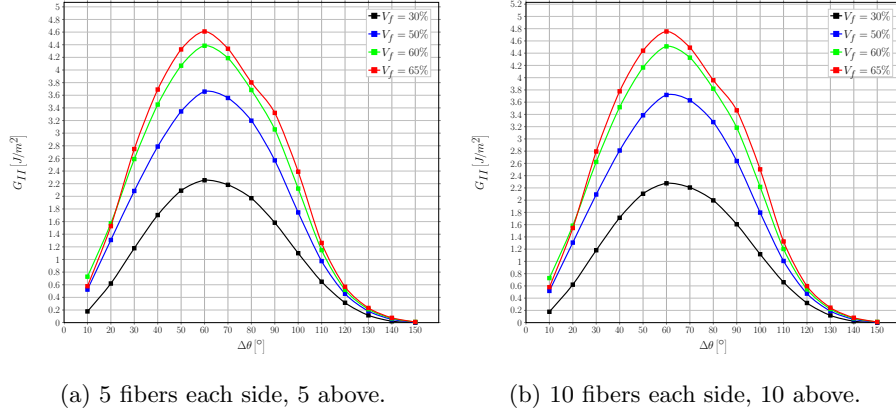


Figure 7: A view of the effect of fiber volume fraction on Mode II ERR in two exemplificative models.

3.2. Interaction between debonds in UD laminates with a single layer of fibers

We start with a simpler (1 parameter: number of fibers in the horizontal directions) but more extreme model: one line of fibers. What's the effect on G_I and G_{II} ? It increases them: a compliant element in the middle of two stiffer ones. Reference to Kies strain magnification. G_I in Fig. 8, G_{II} in Fig. 9.

One graphic for each V_f (30%,50%,60%,65%), one curve for each case of fibers on the side (1, 2, 3, 5, 10, 50, 100).

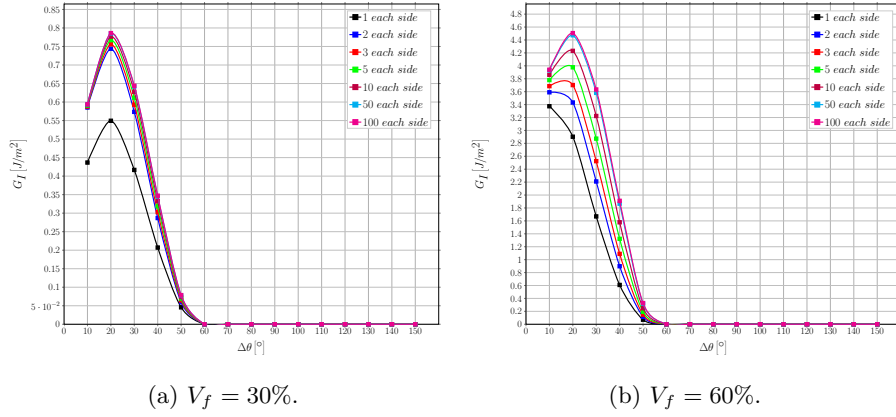


Figure 8: Effect of the interaction between debonds appearing at regular intervals on Mode I ERR in a single-ply laminate with a single layer of fibers at different levels of fiber volume fraction V_f .

3.3. Influence of layers of fully bonded fibers on debond's growth in a centrally located line of debonded fibers

We then move to a ply with multiple lines of fibers and only debonded fibers in the central one (still only 1 parameter: number of fibers in vertical direction, but bit closer to real plies). No significant effect. G_I in Fig. 10, G_{II} in Fig. 11.

One graphic for each V_f (30%,50%,60%,65%), one curve for each case of fibers on top (1, 2, 3, 5, 10, 50, 100).

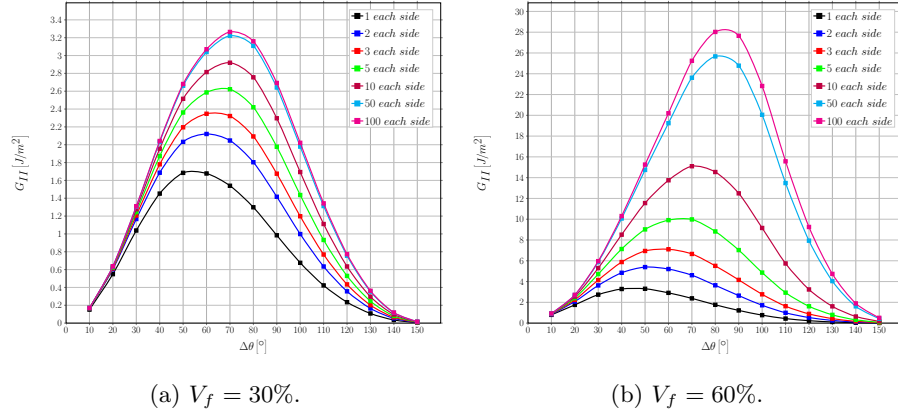


Figure 9: Effect of the interaction between debonds appearing at regular intervals on Mode II ERR in a single-ply laminate with a single layer of fibers at different levels of fiber volume fraction V_f .

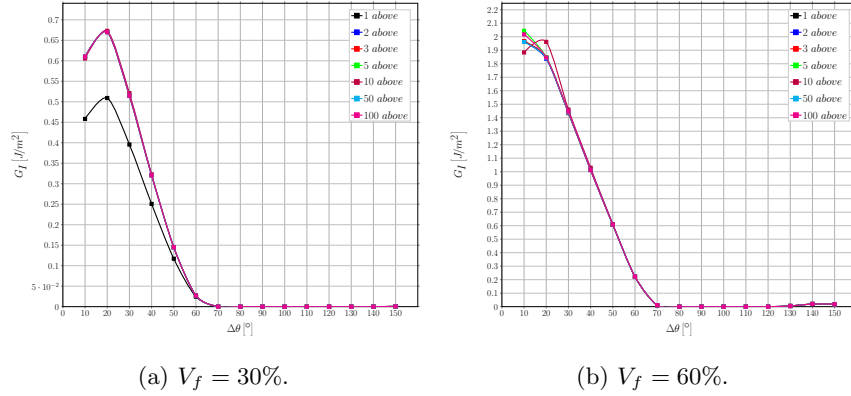


Figure 10: Influence of layers of fully bonded fibers on debond's growth in Mode I ERR in a centrally located line of debonded fibers at different levels of fiber volume fraction V_f .

3.4. Interaction between debonds in UD laminates with multiple layers of fibers

160 Finally models that are closer to real laminates and are more complex (2 parameters: number of fibers along the horizontal direction, number of layers in the vertical one). G_I in Fig. 12, G_{II} in Fig. 13.

One graphic for each V_f (30%,50%,60%,65%), one curve for some selected case of fibers on top and on the side. Hypothesis of selected cases ([n. on side, 165 n. on top]): [1,1], [2,1], [2,2], [5,1], [5,5], [10,1], [10,10], [50,1], [50,10], [100,1],

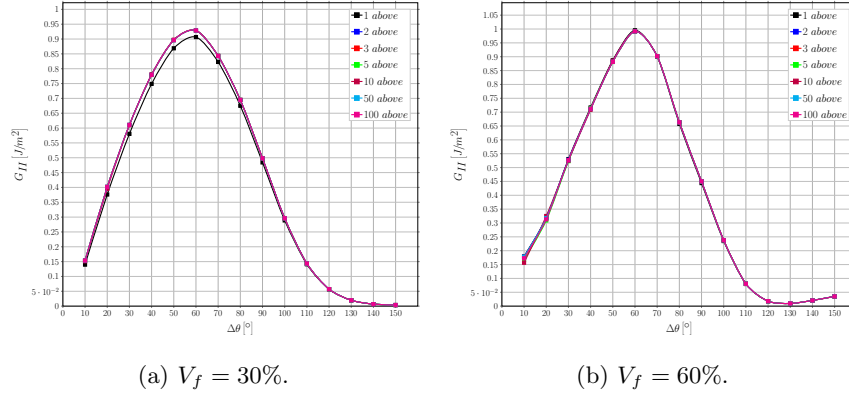


Figure 11: Influence of layers of fully bonded fibers on debond's growth in Mode II ERR in a centrally located line of debonded fibers at different levels of fiber volume fraction V_f .

[100,10]

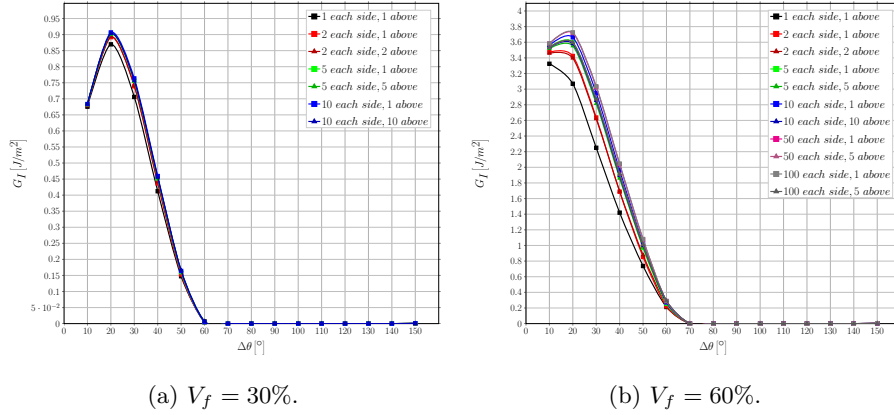


Figure 12: Effect of the interaction between debonds appearing at regular intervals on Mode I ERR in a single-ply laminate with multiple layers of fibers at different levels of fiber volume fraction V_f .

3.5. Comparison with the single fiber model with equivalent boundary conditions

We compare the previous results with the corresponding models of single fibers with equivalent BC. We draw conclusions on the possibility of using a single fiber with equivalent BCs. By remembering the actual ply configurations

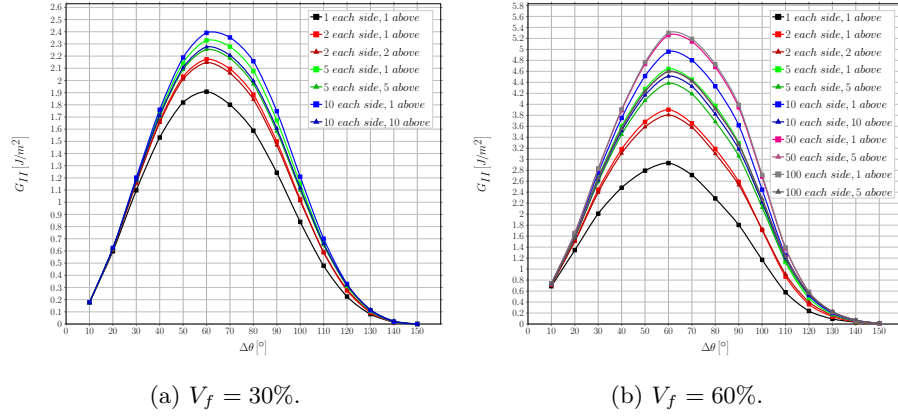
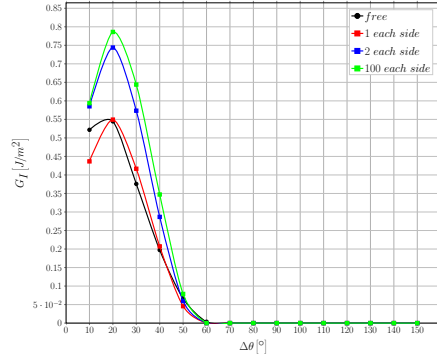


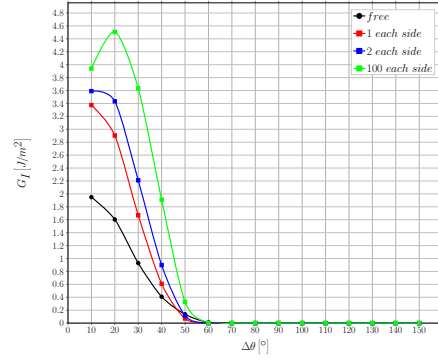
Figure 13: Effect of the interaction between debonds appearing at regular intervals on Mode II ERR in a single-ply laminate with multiple layers of fibers at different levels of fiber volume fraction V_f .

the repeating elements are modeling, and observing that in the vertical direction no significant effect related to the presence of debonded or bonded fiber can be found, we conclude that debonds appearing in fibers aligned in the vertical direction are energetically equivalent, and thus different configurations of debonded/bonded fibers along the vertical direction have the same probability. It is thus likely, from the energetic point of view, that debonds form at the same time along fibers aligned vertically. G_I in Fig. 14 and Fig. 16, G_{II} in Fig. 15 and Fig. 17.

One graphic for each V_f (30%,50%,60%,65%), one curve for single fiber with BC + some selected case of fibers on top and on the side. Hypothesis of selected cases ([n. on side, n. on top]): [1,1], [2,1], [2,2], [5,1], [5,5], [10,1], [10,10]

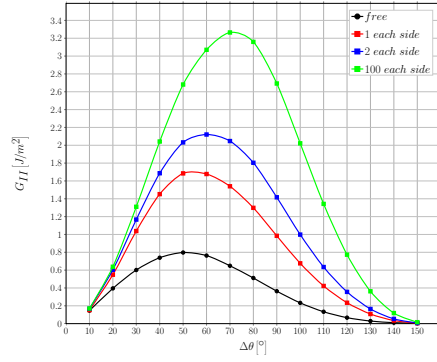


(a) $V_f = 30\%$.

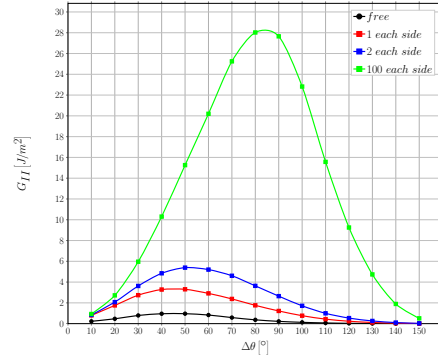


(b) $V_f = 60\%$.

Figure 14: Comparison of Mode I ERR between the single fiber model with free upper boundary and the multiple fibers model with fibers only on the side at different levels of fiber volume fraction V_f .



(a) $V_f = 30\%$.



(b) $V_f = 60\%$.

Figure 15: Comparison of Mode II ERR between the single fiber model with free upper boundary and the multiple fibers model with fibers only on the side at different levels of fiber volume fraction V_f .

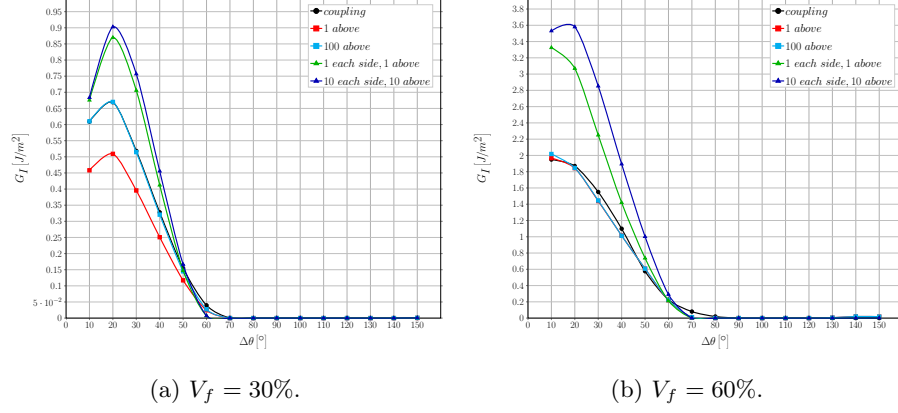


Figure 16: Comparison of Mode I ERR between the single fiber model with coupling conditions along the upper boundary and the multiple fibers model with fibers above and both above and on the side at different levels of fiber volume fraction V_f .

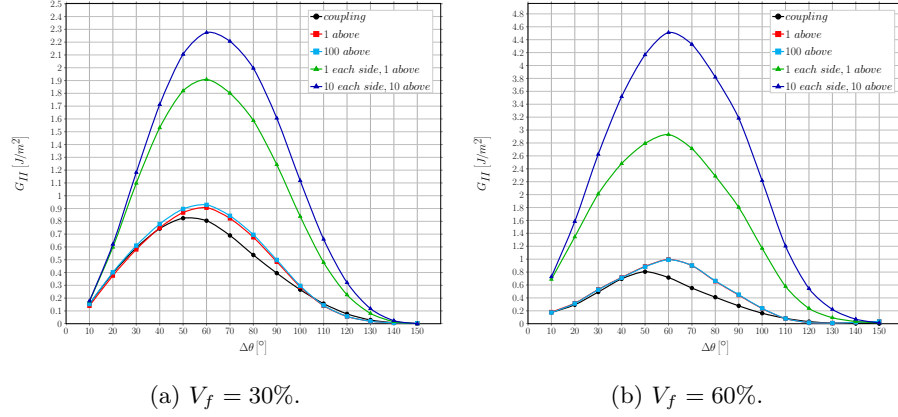


Figure 17: Comparison of Mode II ERR between the single fiber model with coupling conditions along the upper boundary and the multiple fibers model with fibers above and both above and on the side at different levels of fiber volume fraction V_f .

4. Conclusions & Outlook

185 Acknowledgements

References

- [1] Simulia, Providence, RI, USA, ABAQUS/Standard User's Manual, Version 6.12 (2012).

- [2] R. Krueger, Virtual crack closure technique: History, approach, and applications, Applied Mechanics Reviews 57 (2) (2004) 109. doi:10.1115/1.1595677.
190 URL <https://doi.org/10.1115/1.1595677>
- [3] J. R. Rice, A path independent integral and the approximate analysis of strain concentration by notches and cracks, Journal of Applied Mechanics 35 (2) (1968) 379. doi:10.1115/1.3601206.
195 URL <https://doi.org/10.1115/1.3601206>
- [4] C. Sandino, E. Correa, F. París, Numerical analysis of the influence of a nearby fibre on the interface crack growth in composites under transverse tensile load, Engineering Fracture Mechanics 168 (2016) 58–75. doi:10.1016/j.engfracmech.2016.01.022.
200 URL <https://doi.org/10.1016/j.engfracmech.2016.01.022>